ELSEVIER

15 February 1996

Optics Communications 124 (1996) 9–15

OPTICS COMMUNICATIONS

Imaging of biological samples by a collection-mode photon scanning tunneling microscope with an apertured probe

Masayuki Naya [a,b], Shuji Mononobe [a], R. Uma Maheswari [a], Tosiharu Saiki [a], Motoichi Ohtsu [a,c]

[a] *Kanagawa Academy of Science and Technology, KSP East Rm408,3-2-1, Sakado, Takatsu-ku, Kawasaki-shi, Kanagawa-ken, 213, Japan*

[b] *Fuji Photo Film Co., Ltd. Miyanodai Technology Development Center, 798, Miyanodai, Kaisei-machi, Ashigarakami-gun, Kanagawa, 258, Japan*

[c] *Interdisciplinary Graduate School of Science and Engineering, Tokyo, Institute of Technology, 4259 Nagatsuta, Midori-ku, Yokohama 226, Japan*

Received 2 May 1995; revised version received 3 October 1995

Abstract

We report on high resolution imaging by a collection-mode photon scanning tunneling microscope (c-mode PSTM). In our PSTM system, we have used a novel probe with a nanometric protrusion formed from a metal coated sharpened fiber. By using this probe, flagellar filaments of salmonella of diameter 25 nm could be imaged to have a full width at half maximum of 50 nm. Obtained images strongly depended on the separation of the sample to the probe, the diameter of the aperture, and polarization of the irradiated light. Comments on the origins of these dependencies are given.

1. Introduction

A photon scanning tunneling microscope (PSTM), (alternatively called scanning tunneling optical microscope (STOM), near-field scanning optical microscope (NSOM) or scanning near-field optical microscope (SNOM)), based on the short-range electromagnetic interaction between a small dielectric tip and a sample via an induced evanescent field has been recently developed. Because of the possibility of realizing nanometric resolution without any special sample processing, many applications have been proposed [1,2].

The PSTM technique is commonly implemented in two modes. One is illumination mode (i-mode) which uses an evanescent field generated on a nano-aperture to illuminate the sample [3]. By this mode super resolution beyond the diffraction limit is realized due to the sub-wavelength diameter of the aperture. High contrast can be obtained in this mode which paves a way to perform a variety of experiments [4–6]. However additional auxiliary servo-control technique using, e.g., shearing force, has to be used for maintaining the sample-probe separation constant, which makes the instrument complicated and sometimes damages the sample surface. Furthermore, the polarization-state of the emitted evanescent field depends on the shape of the apertured probe in a complex manner. The other scheme is the collection-mode (c-mode) using a nanometric dielectric tip as a scatterer [1] of the non-radiative evanescent field. Usually the evanescent field can be easily generated on the sample surface by irradiating it with the propagating light under the condition of total reflection [7–9]. Since the scattered light intensity decreases rapidly with increasing sample-probe separation, the

SSDI 0030-4018(95)00644-3

separation can be maintained constant by a simple servo-control loop using only conventional collection optics. This is an outstanding instrumental advantage of this mode. Furthermore, the capability of controlling the polarization state of the incident light makes the analysis and evaluation of the observed images simpler. However, in spite of these advantages experimental results with high resolution c-mode PSTM have not yet been fully documented and we believe this can be mainly due to un-matured fabrication technique of a nanometric probe tip.

In this paper, we demonstrate high resolution imaging experiments by the c-mode PSTM with a novel type of nano-apertured probe. To evaluate the performance of the microscope, we used straight-type flagellar filaments of salmonella (FFS) with diameter of 25 nm, as a reference sample. Dependence of the image characteristics on operation parameters such as sample-probe separation, tip size, and polarization state of the incident light have been investigated.

In section 2 we describe the probe, experimental system and the sample, section 3 gives a discussion of the experimental results and finally section 4 gives a summary.

2. Experiments

For detecting only the high spatial-Fourier frequency components of the evanescent field to realize high resolution, a probe with a small dielectric tip is indispensable. To realize such a tip, we have developed a highly reproducible technique. By means of this technique, a probe whose nanometer sized fiber tip protruding out from a gold film (see Fig. 1a) [10] could be fabricated. The fabrication processes can be summarized as: (i) An optical fiber was sharpened to have a tip with a curvature diameter smaller than 10 nm by using the selective chemical etching technique [11–13]. (ii) The sharpened fiber was coated with a gold film of about 150 nm thickness. Because the optical skin depth of gold is about 30 nm, this thickness was sufficient to block the unwanted propagating light. (iii) The gold coated sharpened fiber was dipped into a resin solution (METAL PRIMER, Gunze Sangyo Inc.) and immediately taken out. Due to the surface tension of the resin solution, only the top of the sharpened fiber protrudes out from the resin film. (iv) Next, by dipping it in a KI

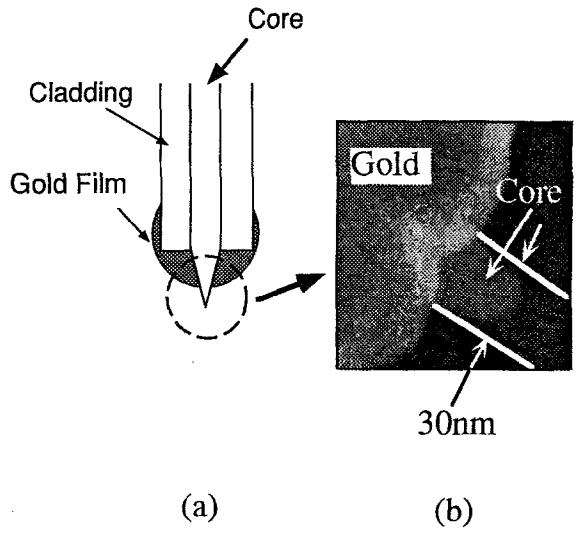

Fig. 1. (a) Schematic of apertured fiber probe. (b) SEM image of probe tip. The diameter at the foot of the protruded fiber is found to be 30 nm.

solution ($KI:I_2:H_2O = 20:1:24000$) to remove the gold film, only gold film protruding out from the resin was removed, because resin film acts as a guard layer for the gold film. Fig. 1b shows a SEM image of the apertured probe. Although the diameter at the foot of the protruded fiber is found to be 30 nm from this figure, its real value should be even smaller because the protruded fiber can be buried in the contamination at the stage of SEM observation. (For this contamination, see Fig. 1 of Ref. [12]). Furthermore, the effective aperture diameter governing the resolution of the PSTM can be even smaller because the high spatial-Fourier frequency components of the evanescent field are preferably scattered at the protruded fiber tip.

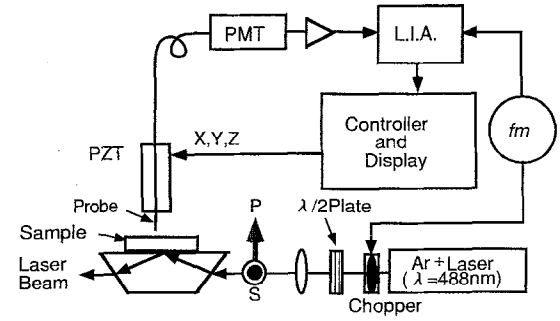

Fig. 2. Experimental system of the c-mode PSTM. A half wavelength plate is used to control the polarization state of the incident light.

Fig. 2 shows the experimental system of the c-mode PSTM. An Ar^+ laser with a wavelength of 488 nm was used as a light source, and a half wavelength plate was installed for adjusting the polarization state of the incident light. A thin glass plate was used as a substrate for the sample and was fixed on a glass prism with index matching oil. The laser beam was made incident into the prism under the condition of total reflection. The evanescent field generated on the sample surface was scattered and picked up by the optical fiber probe. The probe is set on a PZT tube to scan in the *XYZ* direction. A photomultiplier and a lock-in amplifier were used for the phase sensitive detection. A commercial AFM controller (Seiko Instruments Inc.; SPA3700) was used for scanning and image processing.

The probe was scanned under constant-height mode. Rapidly decreasing optical power from the substrate was used to set the initial height of the probe. In order to compensate for the effects of the tilts substrate, we have carefully adjusted the time constant of the servo control loop. The response time of the controller was shorter than 0.1 s, and scanning frequency was 2 Hz for a scanning length of 5 μm. Therefore this feed back control loop does not respond to sample features of size smaller than 1 μm.

Straight-type flagellar filaments of salmonella (FFS) were used as the reference sample for evaluating the performance of the c-mode PSTM. The FFS has been popularly known as a molecular motor [14], and thus, its size and structure have been well calibrated. The FFSs were fixed on a hydrophilized glass plate. Fig. 3 shows an image of FFSs observed by a transmission electron microscope (TEM), from which the diameter of the FFS was measured to be 25 nm.

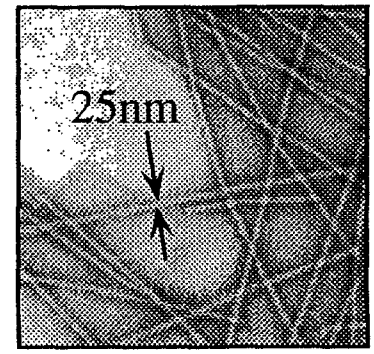

Fig. 3. TEM image of the straight-type flagellar filaments of salmonella (FFS) provided by S.-I. Aizawa. The diameter of each filament was 25 nm, which was confirmed by images taken by a transmission electron microscope.

3. Results and discussion

Fig. 4a is a PSTM image of the FFSs when the incident light was s-polarized, i.e., the electric field vector lies in the substrate surface plane. The fiber probe shown by Fig. 1b was used for this imaging. Scanning area is 5 μm × 5 μm with the corresponding number of pixels being 256 × 256. Therefore the size of one pixel is about 20 nm × 20 nm. For this scan, the sample-probe separation was estimated to be less than 15 nm, and this was estimated in the following way: After finishing this scan, the probe was approached towards the sample by applying a voltage corresponding to a distance of 15 nm to the PZT. At this position, when the scanning process was repeated, we observed streaks in the image due to the probe scratching the sample surface.

Fig. 4a shows that FFSs fixed perpendicular to the direction of the incident beam (see the arrow in the figure) were clearly imaged with high contrast. Fig. 4b shows a cross-sectional profile of the detected signal intensity for the part identified by a white bar in Fig. 4a. This profile was obtained by performing averaging 100 lines along the orientation shown by white line. The bright region corresponds to filament of FFS while the dark region on either sides of the bright region corresponds to "shadow" formed by the short range electromagnetic interaction between the probe tip, the filament and the substrate. The full width at half maximum (FWHM) of the bright region is 50 nm which corresponds to the diameter of FFS. Such a smaller value, suggests for a high resolution capability of the present system. This was used by the fact that the high-spatial Fourier frequency components are selectively picked up by the fiber tip protruding out of the gold film [15]. However, for accurate estimation of resolution, the definition of resolution is required. Furthermore it should be noted that this experimental result is still preliminary because the pixel size is larger than the size of probe tip and is as large as the FFS diameter. Smaller FWHM, i.e., higher resolution, is expected by reducing the pixel size.

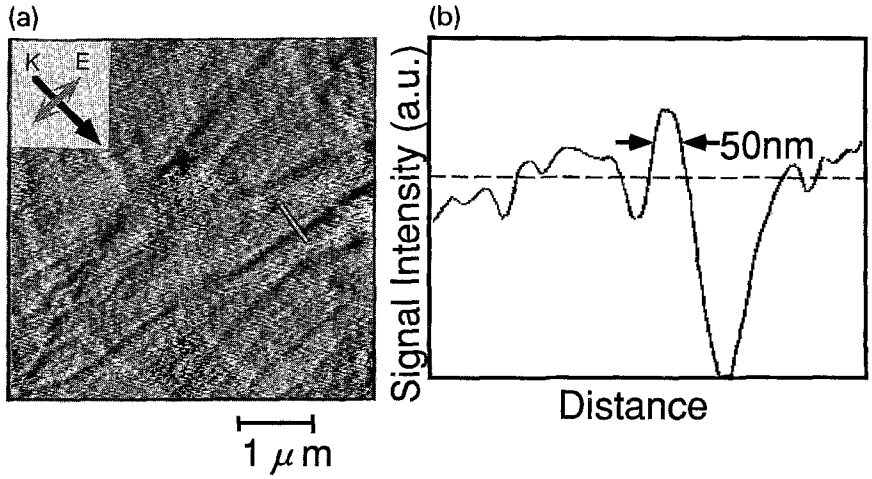

Fig. 4. (a) A PSTM image of the FFSs for the s-polarized incident light. The sample-probe separation was about 15 nm. Black and gray arrows represent the direction of the wave vector k of the incident light and gray arrow indicates the electrical field E respectively. (b) A cross-sectional profile of the detected signal intensity for the part identified by a white bar in (a). This profile was obtained by performing averaging 100 lines, along the orientation shown by the white line. The full width at half maximum (FWHM) of the bright region is 50 nm which corresponds to the diameter of FFS.

Fig. 5 shows an image taken under the same condition as Fig. 4a, except for the sample-probe separation being increased to 65 nm. Almost the same image was obtained, except that the FWHM of the cross-sectional profile of he detected signal intensity of image was increasel to about 150 nm. This dependency of the size of the images on the sample-probe separation can be resulting from the confinement characteristics of the evanescent field, i.e., the penetration depth of the evanescent field is of the order of the sample size. In other words, the decay length of higher spatial frequency component of the evanescent field is shorter [15]. Therefore, for efficient pick up, the probe must be brought closer to the sample.

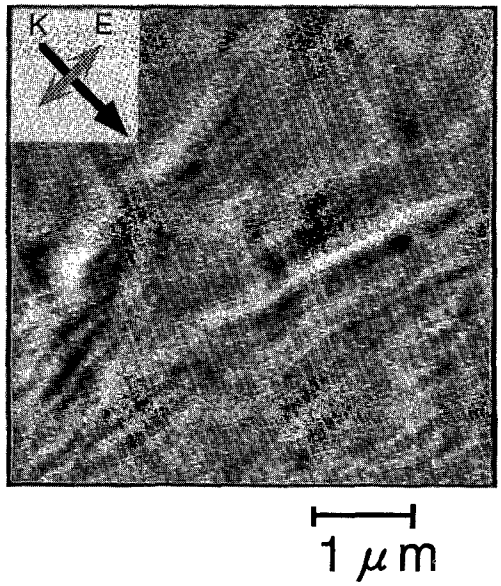

Fig. 5. A PSTM image taken under the same conditions as of Fig. 4a, except for the sample-probe separation being increased to 65 nm.

In order to study the dependence of the pick up efficiency on sample-probe separation more quantitatively, the spatial Fourier spectrum of the images obtained under a separation of 15 nm and 65 nm shown respectively in Figs. 4a and 5 were calculated. For an exact estimation, the whole data, containing many FFSs, were used for the calculation. Results are shown in Fig. 6, and comparing the two curves in this figure, it can be seen that the strength of the high spatial frequency component decreases with increasing sample-probe separation. This supports the theory of confinement of high frequency components in the previous paragraph.

Fig. 7 shows the PSTM image of the same sample obtained by using a probe tip with an aperture diameter as large as 100 nm. The sample-probe separation was fixed to be less than 15 nm. Comparison with Fig. 4a confirms that the image suffers also a kind of defocusing. The origin of this defocusing is straight forward,

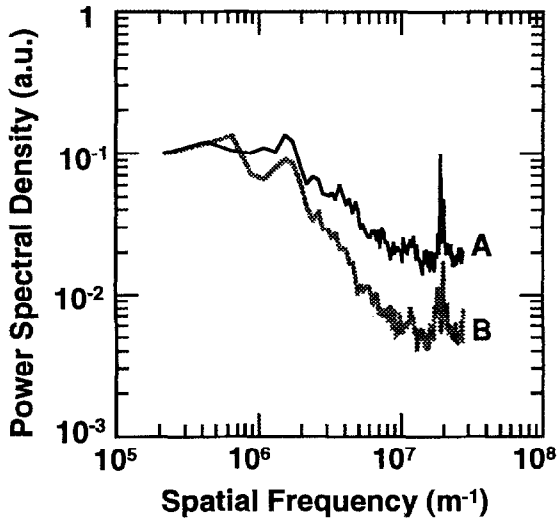

Fig. 6. The spatial Fourier spectrums of PSTM images for sample-probe separations of (A) 15 nm (corresponding to Fig. 4a) and (B) 65 nm (corresponding to Fig. 5).

i.e., the lower spatial frequency components were effectively picked up by the larger aperture [15].

As a next step for evaluating the performances of the c-mode PSTM, the dependency of the image on the vectorial property of the light field was studied. Fig. 4a is taken when the incident light was s-polarized. Fig. 8a shows the PSTM image for exactly the same scanned area as that of Fig. 4a taken when the incident light was p-polarized, i.e., the electric field vector is normal to the substrate surface. This image was apparently different from the image of Fig. 4a. Fig. 8b shows a cross-sectional profile of the detected signal intensity for the part identified by a white bar in Fig. 8a. This profile was obtained by performing averaging 100 lines along the orientation shown by white line. Here, in contrast to that of Fig. 4b the bright areas can be seen on both sides of the sample. This difference can be explained by considering the distributions and directions of the optically induced dipoles on the sample surface and the probe tip, where the evanescent field mediates the short-range electromagnetic interaction between the sample and the probe tip [16]. Figs. 9a and 9b explain the origin of this difference depicting the schematic view of the induced dipoles on the sample surface and probe tip, and the electric lines of force of the evanescent field. In the case of s-polarization, as shown in Fig. 9a, the direction of the dipole, induced on the sample surface are in parallel to the substrate surface plane. Thus, the lobes of electric lines of force of the evanescent field is generated above the sample. Since the dipole induced on the probe tip by this evanescent field lies along the lines of electric force of this lobe, it is in parallel to the substrate surface plane when the probe tip is just above the sample. The wave vector of the scattered propagating light, generated by this dipole, is thus, inparallel to the probe axis, which is most efficiently coupled to the guided mode of the fiber. This coupling efficiency is always lower when the probe tip is deviated from this position. This is the reason for the single intensity peak detected seen in the cross sectional profile as Fig. 4a.

On the other hand, since the direction of the dipole on the sample, induced by the p-polarized light, is perpendicular to the substrate surface, the lobes of the generated evanescent-field are on both sides of the sample. Thus, when the probe tip is just above the sample, the direction of the induced dipole is also perpendicular to the substrate. The wave-vector of the scattered light is, then, perpendicular to the probe axis, which gives the lowest coupling efficiency to the guided mode of the fiber. Therefore, the cross sectional light intensity shows two peaks.

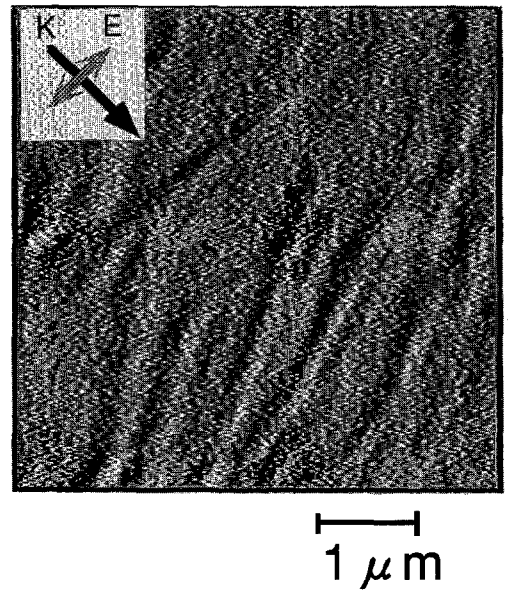

Fig. 7. A PSTM image of the FFS obtained by using a probe tip with an aperture diameter as large as 100 nm. Sample-probe separation is about 15 nm.

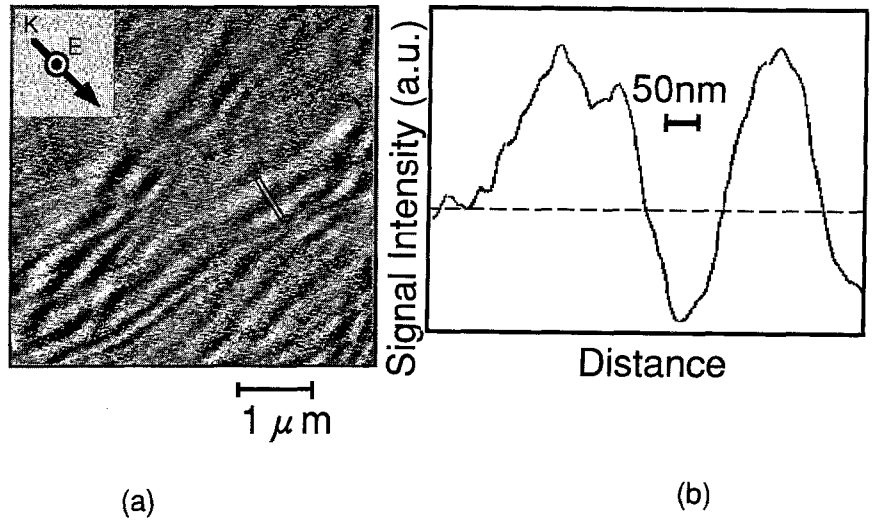

Fig. 8. (a) A PSTM image for exactly the same scan area and the same conditions as that of (a), when the incident light was p-polarized. (b) A cross-sectional profile of the detected signal intensity for the part identified by a white bar in (a). This profile was obtained by performing averaging 100 lines along the orientation shown by white line.

4. Summary

This paper demonstrated the capability of high resolution imaging by a c-mode PSTM with a nano-apertured probe. The system could be operated under all optical mode without any auxiliary control by taking advantage of the exponential dependence of the evanescent field intensity. High resolution imaging of flagellar filament of salmonella of nominal diameter of 25 nm was carried out and the observed image had the FWHM of 50 nm. The dependencies of the image on the sample-probe separation, and diameter of the aperture were studied. It has been confirmed that the probe tip picks up the evanescent field that is confined to the nanometric sample with penetration depth corresponding to the sample size. We also observed the dependency of the image on the polarization state of incident light, and this result was explained in terms of the lirection of the induced dipole in the near-field region.

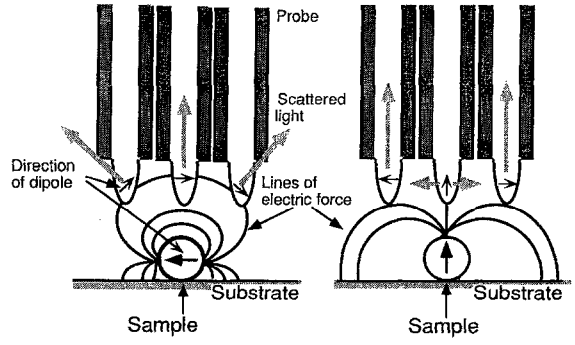

Fig. 9. Illustrations of the directions of the lines of electric force of the evanescent field and the direction of scattered light by dipole of the optical fiber probe. (a) For the s-polarized incident light. (b) For the p-polarized incident light.

Acknowledgements

The authors wish to thank Prof. S. Aizawa at Teikyo Univ. for providing the flagellar filaments of salmonella, and Dr. M. Sano of T.I.T. for providing software to perform the spatial Fourier spectral analysis of the PSTM images.

References

[1] D.W. Pohl and D. Courjon, eds., Near field optics, NATO ASI series E, Vol. 242 (Kluwer, Dordrecht, 1993).
[2] M. Ohtsu, J. Lightwave Tech. 13 (1995) 1200.
[3] D.W. Pohl, W. Denk and M. Lantz, Appl. Phys. Lett. 44 (1984) 651.

[4] E. Betzig and J.K. Trautman, Science 10 (1992) 189.
[5] E. Betzig, J.K. Trautman, J.S. Weiner, T.D. Harris and R. Wolfe, Appl. Optics 22 (1992) 4563.
[6] J.K. Trautman, E. Betzig, J.S. Weiner, D.J. DiGiovanni, T.D. Harris, F. Hellman and E.M. Gyorgy, J. Appl. Phys. 15 (1992) 4659.
[7] D. Courjon, K. Sarayaddine and M. Spajer, Optics Comm. 71 (1989) 23.
[8] S. Jiang, N. Tomita, H. Ohsawa and M. Ohtsu, Jpn. J. Appl. Phys. 30 (1991) 2107.
[9] S. Jiang, H. Ohsawa, K. Yamada, T. Pangari-Buan, M. Ohtsu and K. Imai, Jpn. J. Appl. Phys. 7 (1992) 241.
[10] S. Mononobe, M. Naya, R. Uma Maheswari, T. Saiki, M. Ohtsu, NFO-3, EOS-Topical Meeting, 8 (1995) 105.
[11] T. Pangaribuan, K. Yamada, S. Jiang, H. Ohsawa and M. Ohtsu, Jpn. J. Appl. Phys. 9A (1992) L1302.
[12] T. Pangaribuan, S. Jiang and M. Ohtsu, Electron. Lett. 22 (1993) 1978.
[13] T. Pangaribuan, S. Jiang and M. Ohtsu, Scanning 16 (1994) 362.
[14] S. Kato, H. Okino, S.-I. Aizawa and S. Yamaguchi, J. Mol. Biol. 219 (1991) 471.
[15] H. Hori, Near Field Optics, NATO ASI series E, Vol. 242 (Kluwer, Dordrecht, 1993) p. 105.
[16] B. Labani and C. Girard, J. Opt. Soc. Am. B 6 (1990) 936.